ISSN 1068-3372, Journal of Contemporary Physics (Armenian Academy of Sciences), 2025, Vol. 60, No. 2, pp. 210–221. © Pleiades Publishing, Ltd., 2025.
Russian Text © The Author(s), 2025, published in Izvestiya Natsional'noi Akademii Nauk Armenii, Fizika, 2025, Vol. 60, No. 2, pp. 252–268.

Thin Films of CdS Formed on a Polyimide Substrate by Chemical Bath Deposition Method

S. G. Petrosyan[a], A. S. Musayelyan[a, *], A. S. Tokmajyan[a], V. F. Gremenok[b], A. V. Stanchik[b], K. P. Buskis[b], and O.V. Korolik[c]

[a] *Institute of Radiophysics and Electronics, NAS of Armenia, Ashtarak, Armenia*

[b] *State Scientific and Production Association "Scientific and Practical Center of the NAS of Belarus for Materials Science", Minsk, Belarus*

[c] *Belarusian State University, Minsk, Belarus*

*****e-mail: ashmusa@mail.ru*

Received April 16, 2025; revised May 6, 2025; accepted May 26, 2025

Abstract—Thin films of polycrystalline cadmium sulfide (CdS) were deposited on polyimide substrates using the chemical bath deposition method at a fixed solution temperature of (62 ± 1)°C. The influence of deposition time on the structural and optical properties of the resulting thin films was studied in detail. X-ray diffraction (XRD) revealed that the films predominantly consist of the hexagonal phase of CdS, with a crystallite size of approximately 10 nm, which slightly decreases with increasing deposition time. The surface roughness of the films was measured using atomic force microscopy. Scanning electron microscopy showed a uniform, compact, and smooth film surface. Raman measurements revealed three main peaks corresponding to the 1LO, 2LO, and 3LO modes in CdS. Optical measurements showed a high transmittance coefficient (~85%) and a low reflectance coefficient (4–7%) in the spectral range of 520–1000 nm. Due to changes in the stoichiometry of the CdS films, the optical band gap varied within the range of 2.30–2.37 eV with increasing deposition time. Room temperature photoluminescence spectra of the films exhibited two emission peaks located at 500 nm (2.49 eV) and 708 nm (1.75 eV), which can be attributed to free carrier recombination and excitonic or radiative transitions involving donor and acceptor levels, respectively. The obtained results demonstrate that by controlling only the deposition time, it is possible to deposit CdS thin films on polymer substrates at a relatively low chemical bath temperature. These films, without any post-growth treatment, possess sufficiently good physical properties, making them suitable for use in various flexible optoelectronic devices.

Keywords: thin film CdS, Chemical Bath Deposition (CBD), flexible substrate, XRD, AFM, Raman

DOI: 10.1134/S1068337225700549

1. INTRODUCTION

Recently, cadmium sulfide (CdS) thin films have attracted the attention of researchers due to their fairly good optical and electronic properties, as well as high chemical stability [1]. In most cases, CdS is an *n*-type semiconductor, with conductivity resulting from intrinsic donor defects such as sulfur (S) vacancies and cadmium (Cd) interstitial atoms. CdS is characterized by a wide direct band gap of approximately 2.4 eV at room temperature. This compound is considered one of the most promising materials for thin-film solar cells, serving as a wide-bandgap window layer in combination with absorber layers such as cadmium telluride (CdTe), copper indium gallium sulfide (or selenide) (CIGS(Se)), kesterites (CZTS), or perovskites [2].

Various physical and chemical deposition methods can be used to obtain CdS thin films, including electrodeposition [3], chemical bath deposition (CBD) [4–6], thermal evaporation [7], chemical vapor deposition (CVD) [8], pulsed laser deposition [9], RF magnetron sputtering [10], close-spaced sublimation [11], metal-organic chemical vapor deposition (MOCVD) [12], chemical pyrolysis [13], and others. Among these technologies, the CBD method offers several advantages for growing CdS thin films, including low cost, environmental friendliness, high purity, compositional stability of the film, and simplicity of the method. In addition, this method enables growth at relatively low temperatures, making it possible to use inexpensive polymer substrates.

Currently, the deposition of CdS films on polymer substrates such as polyimide (PI) is of great interest [14–17] due to their flexibility, lightweight, low cost, high transparency in the visible light range, high thermal stability (up to 400°C), low coefficient of thermal expansion, and excellent electrical properties.

In this study, CdS thin films were deposited on polyimide (PI) substrates using the chemical bath deposition method at a fixed solution temperature of (62 ± 1)°C [18], but with varying deposition durations. The main goal was to optimize the processing conditions for producing CdS films with improved physical properties, enabling their use as a buffer layer in thin-film solar cells, as well as an active layer in lightweight and flexible optoelectronic devices. The study provides a detailed discussion of the effect of deposition time on the structural, morphological, and optical properties of CdS films deposited on PI substrates.

2. METHODOLOGY AND EXPERIMENTAL DETAILS

2.1. Deposition Process

CdS thin films were deposited on PI substrates using the CBD method, with thicknesses ranging from 40 to 85 nm. The samples were formed in a solution containing 90 mL of deionized water, 30 mL of 25% aqueous ammonia solution, 40 mL of cadmium sulfate (0.0096 M $CdSO_4$) as the cadmium source, and 40 mL of thiourea (0.8 M $CS(NH_2)_2$) as the sulfur source. The pH of the resulting solution was 10.7. The CdS layer was grown on PI substrates, which were vertically immersed in the prepared solution, at an experimentally determined optimal temperature for stable CdS layer deposition of (62 ± 1)°C. Throughout the entire deposition process, the solution was stirred using a magnetic stirrer.

The substrates were pre-cleaned using ultrasound in acetone and ethanol, then rinsed with deionized water and dried with a stream of nitrogen. After deposition, the CdS films were rinsed in an ultrasonic bath for 10 minutes to remove any adhering CdS particles and then dried with a stream of nitrogen. Three series of CdS films were obtained: CdS: CS5, CS10, and CS15, corresponding to deposition times of 5, 10, and 15 min, respectively.

2.2. Methods for Studying Thin Films

Due to the flexibility of the PI substrate, measuring the thickness of thin films using optical methods or a profilometer presents certain difficulties and uncertainties. Therefore, the thickness of the CdS films was estimated based on SEM cross-sectional images of the thin films deposited on the substrates. The obtained thickness values for the CS5, CS10, and CS15 samples were 46.2, 62.8, and 82.7 nm, respectively.

Various analytical methods were used to characterize the deposited CdS films. The crystal structure was examined using an Ultima IV X-ray diffractometer (Rigaku) with a Cu$K\alpha$ radiation source (λ = 1.5406 Å) in grazing incidence X-ray diffraction (GIXD) geometry, with a grazing angle of 1° and a 2θ range from 20° to 80°.

The elemental composition of the synthesized films was studied using energy-dispersive X-ray microanalysis with an INCA Energy system (Oxford Instruments), offering a resolution of 1.0 μm and a sensitivity of 0.1 at %. Surface and cross-sectional topography were analyzed using a scanning electron microscope (SEM) H-800 813 (Hitachi, Japan) with a resolution of no worse than 0.2 nm. The topographical properties of the films were examined by atomic force microscopy (AFM) using a Solver Nano system (NT-MDT) at a resonance frequency of 227 kHz in semi-contact mode, with a probe tip radius of 10 nm. For each sample surface, at least five areas with a scan size of 5 × 5 μm^2 were selected. For each selected area, the arithmetic average and root mean square roughness values, as well as the maximum height of the surface profile roughness, were determined; the results were then averaged for each sample.

Raman scattering (RS) and photoluminescence (PL) spectra of CdS thin films were recorded at room temperature using a Nanofinder HE confocal spectrometer (LOTIS TII, Belarus–Japan). The measurements were performed in a backscattering geometry without considering the polarization of the scattered radiation. A continuous-wave solid-state laser with a wavelength of 473 nm was used as the excitation source. A 100× objective lens (NA = 0.95) provided an excitation spot size of approximately 0.7 μm. The backscattered light was dispersed using diffraction gratings with 1800 lines/mm (for RS) and 600 lines/mm (for PL), with spectral resolutions of no worse than 1 and 3 cm^{-1}, respectively. Signal detection was carried out using a thermoelectrically cooled CCD array with an integration time of 30 s. To prevent thermal damage to the samples, the incident laser power was set to 64 μW for RS measurements and 24 μW for PL measurements. Transmission and specular reflection spectra of the films at an incident–reflection angle of 8º were measured using a Photon RT spectrophotometer (Essent Optics) with a spectral resolution of no worse than 4 nm, using unpolarized light in the wavelength range of 400–1000 nm.

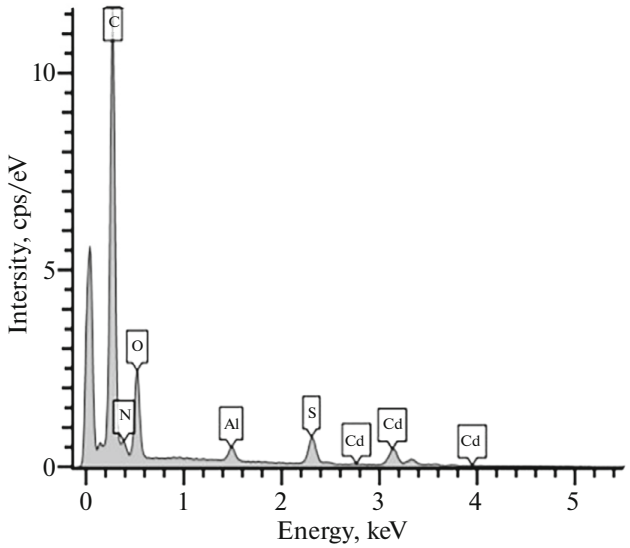

Fig. 1. EDS spectrum of the CS10 thin film deposited on a PI substrate.

3. EXPERIMENTAL RESULTS AND DISCUSSION

The CdS films deposited on PI substrates were transparent with a slight light-yellow tint and had a uniform surface without visible pinholes. The adhesive tape test demonstrated good adhesion of the layers to the substrate surface.

3.1. Elemental Composition Analysis of the Films

The composition of the CdS films after deposition was analyzed using energy-dispersive X-ray spectroscopy (EDS). A typical EDS spectrum, representative of all CdS films obtained at different deposition times, is shown in Fig. 1.

The spectrum shows peaks corresponding to cadmium (Cd), sulfur (S), carbon (C), nitrogen (N), oxygen (O), and aluminum (Al). The presence of C, O, and N is associated with the polyimide substrate. The Al peak is attributed to the sample holder. The atomic concentrations of elements in the deposited films and the variation of the Cd/S ratio with deposition time are presented in Table 1.

It was found that the composition of the films deviates from the stoichiometric ratio, with all films being sulfur-rich. As the deposition time increases (from 5 to 15 min), the atomic concentration of Cd in the CdS films increases significantly, while the sulfur content correspondingly decreases. This suggests the presence of either interstitial atoms or Cd vacancies in the film, which act as acceptors and lead to a reduction in the free carrier concentration due to a high degree of compensation.

3.2. Analysis of SEM Results

To investigate the effect of deposition time on the morphological characteristics of CdS thin films, an analysis of SEM images was conducted. It was found that the duration of the deposition process (5, 10, and 15 min) does not play a significant role in the morphology of the thin films. As an example, Fig. 2 presents SEM images of the surface and cross-sectional views of CdS films deposited for 10 and 15 min, respectively. The micrographs show a dense film structure with a smooth surface that is relatively free of

Table 1. Elemental composition of CdS thin films obtained at different deposition durations

Sample	Cd, at %	S, at %	Cd/S	Compound
CS5	28.26	71.74	0.39	$Cd_{0.56}S_{1.44}$
CS10	43.87	56.13	0.78	$Cd_{0.88}S_{1.12}$
CS15	41.29	58.71	0.70	$Cd_{0.83}S_{1.17}$

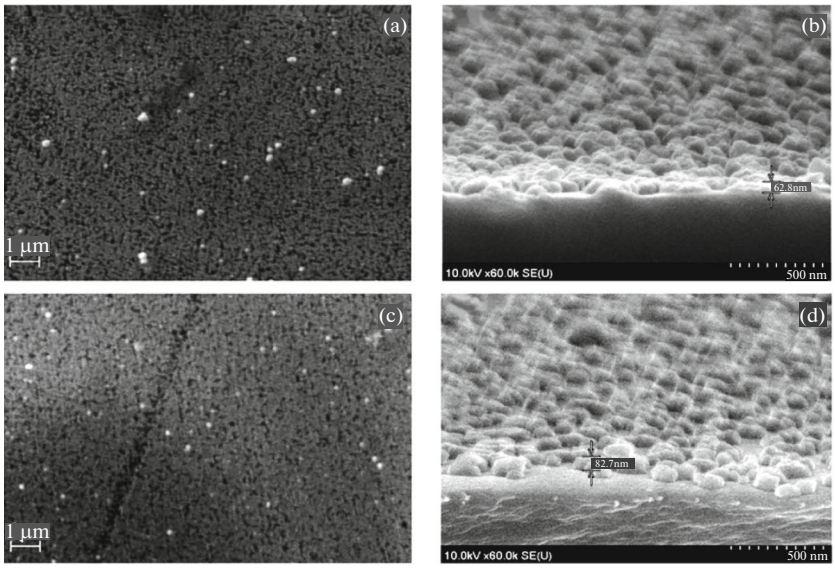

Fig. 2. SEM micrographs and cross-sections of CdS thin films obtained at deposition durations of: (a, b) 10 and (c, d) 15 min.

voids, holes, and cracks. All samples exhibit well-defined spherical grains that are approximately uniform in size, which is attributed to the relatively low deposition rate and the ion-ion film formation mechanism.

The appearance of spherical granules in the SEM image may be attributed to the spheroidal structure of sulfur ions. Meanwhile, the presence of several white, agglomerated particles with well-defined boundaries on the surface of the films, as seen in the SEM image, indicates the presence of sulfur [19, 20].

It should be noted that increasing the deposition time does not have a significant effect on the grain size. In all samples, uniformly distributed nanometer-sized grains evenly cover the substrate surface. The SEM images show that the grains have well-defined boundaries and are size-distributed within the range of 124–132 nm.

3.3. Analysis of AFM Images

AFM is one of the most effective methods for analyzing nanostructured thin films. This technique allows for the determination of various parameters characterizing the film surface, such as grain size, root mean square roughness (R_{rms}), average roughness (R_a), surface profile skewness (R_{sk}), and kurtosis (R_{ku}) [21]. Two-dimensional and three-dimensional AFM images of CdS films on PI substrates are shown in Fig. 3.

In Figs. 3a, 3c, and 3e, the 2D images scanned over an area of 5×5 μm^2 show the presence of spherical particles in all films. The grains grew with various orientations, indicating the polycrystalline nature of the films. The images reveal that the particles are uniformly distributed across the film surfaces, which consist of nanoscale grains. As seen, the deposition time has a significant effect on surface roughness. Various surface topography parameters calculated from the AFM data are presented in Table 2. The obtained values for both average and root mean square roughness indicate that the films exhibit a nanotopographic surface texture.

CdS films grown with a deposition duration of 5 minutes showed a higher R_a value compared to films deposited for longer times. This is likely due to insufficient thermal energy available to the adsorbed atoms for surface diffusion and the formation of a larger number of nucleation centers. As a result, atoms continuously arriving from the solution attach to existing centers, leading to the formation of more hill-like structures during the shorter deposition time, and the films therefore exhibit higher surface roughness. As the deposition time increases, the surface roughness decreases. This may be attributed to the formation of a greater number of nucleation centers over a longer period, promoting the development of a more uniform film on the substrate surface. It is known that the surface roughness parameter called skewness (R_{sk}) characterizes the symmetry of the amplitude distribution function of the surface profile around the mean line, while kurtosis (R_{ku}) characterizes the sharpness of the probability density of the profile amplitude [21].

The R_{sk} value of the deposited CdS films was found to be positive (Table 2), indicating a predominance of valleys over peaks on the film surface, as well as a slight asymmetry in the distribution of peaks along

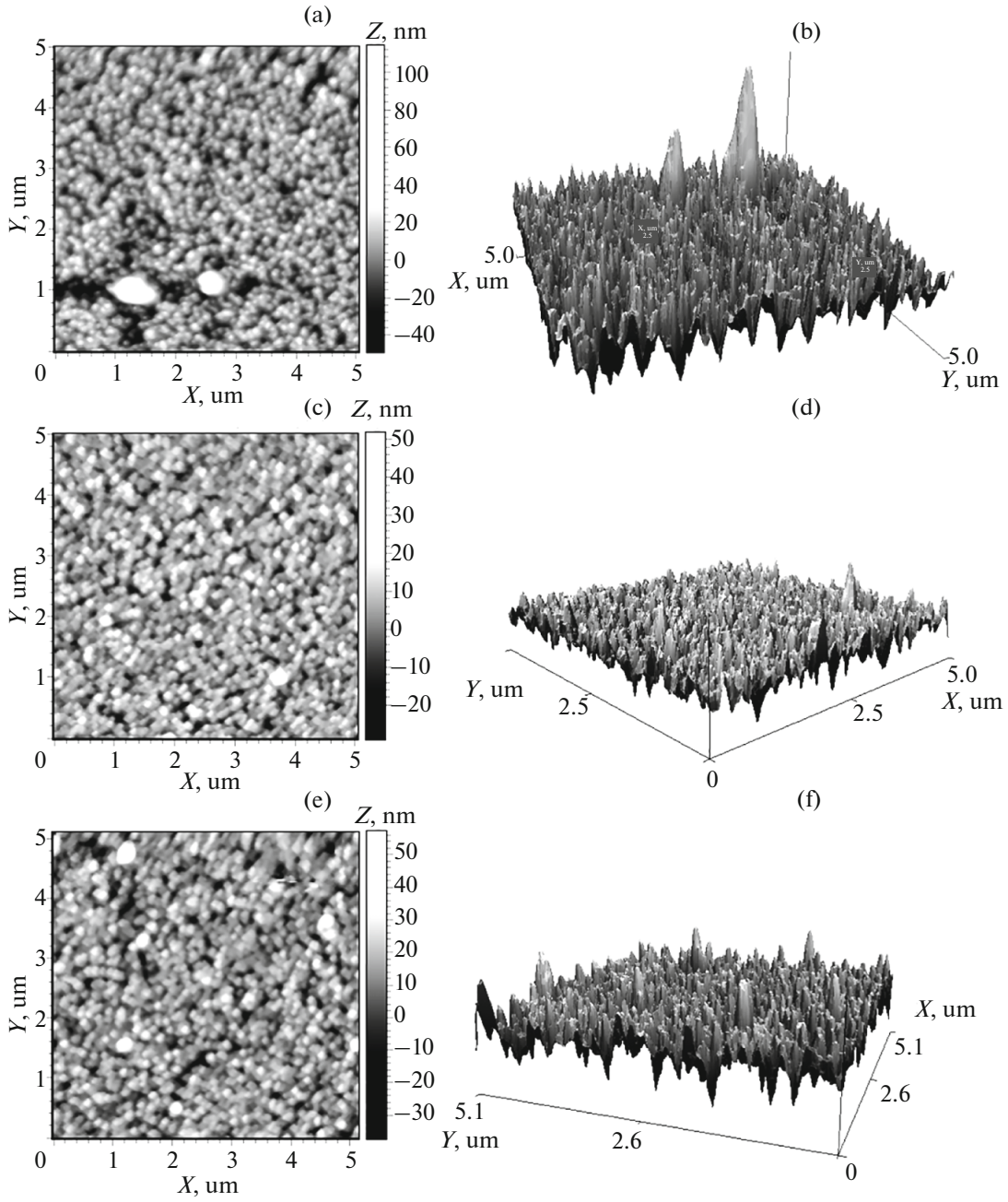

Fig. 3. 2D and 3D AFM images of CdS films obtained at different deposition durations: (a, b) 5 min; (c, d) 10 min; and (e, f) 15 min.

the surface profile. At the same time, the skewness of the profile decreases with increasing deposition time, indicating a change in the height amplitude distribution of the profile from slightly asymmetric to more symmetric. As for kurtosis, when $R_{ku} < 3$, it is considered that the surface contains relatively few high peaks and deep valleys, resulting in an almost flat (platykurtic) surface [21]. If $R_{ku} = 3$, the surface profile is characterized by a Gaussian amplitude distribution (mesokurtic). In our case, for all CdS films deposited on PI substrates, R_{ku} was found to be greater than 3 (Table 2), indicating the presence of relatively many high peaks and shallow valleys in the surface profile (leptokurtic).

It should be noted that increasing the deposition time to 15 min does not result in a noticeable change in the average crystal size. AFM images show that the film surface has a mosaic structure with large surface structural features averaging around 100 nm in size. This value exceeds the average grain size calculated from X-ray diffraction (XRD) data (see below).

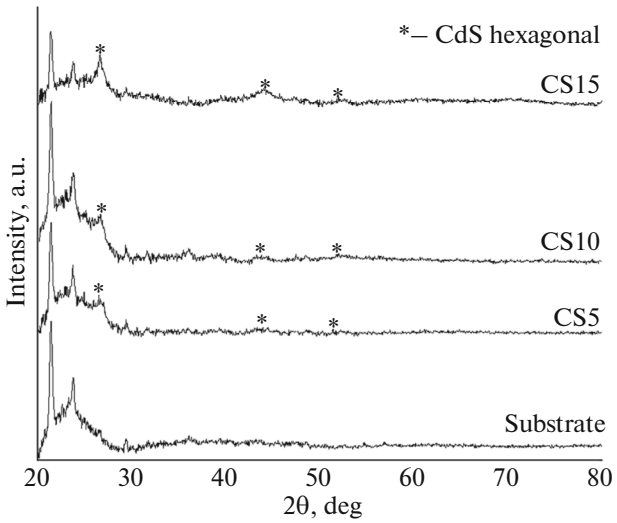

Fig. 4. Diffraction patterns of CdS films depending on deposition time: CS5—5 min; CS10—10 min; CS15—15 min.

It is well known that AFM imaging does not allow for the determination of the average crystallite size obtained from XRD analysis, since in the latter case, the crystallite size is determined based on the smallest crystallites distributed throughout the entire thickness of the film (see below).

3.4. Analysis of XRD Results

Figure 4 shows the diffractograms of the deposited CdS thin films. It can be seen that the X-ray diffraction analysis of various CdS film samples deposited for different durations yields diffractograms of similar appearance.

All diffractograms indicate the polycrystalline nature of the films, with dominant diffraction peaks at angles of approximately 26.6°, 44.4°, and 52.2°. The prominence of the (002) peak suggests that the *c*-axis texture of the wurtzite film is predominantly oriented perpendicular to the substrate surface. The obtained results are in good agreement with previously published literature data [22, 23].

The presence of additional diffraction peaks and the relatively large full width at half maximum (FWHM) of the main (002) peak, approximately 1.2°, indicate a polycrystalline nature with the possible presence of amorphous regions. The results also confirm that CdS films deposited by the CBD method do not require a crystalline substrate to form a highly ordered texture. This conclusion is particularly noteworthy, as the PI substrates were at a relatively low temperature during deposition.

The average crystallite size (L) was calculated using the Scherrer equation [19, 24]:

$$L = (0.9\,\lambda)/\beta\cos\theta, \tag{1}$$

where λ is the wavelength of the incident X-ray radiation ($\lambda = 1.5406$ Å), β is the FWHM of the peak in radians, and θ is the Bragg diffraction angle.

The interplanar spacing (d), lattice parameters (a and c), lattice microstrain (ε), and dislocation density (δ) for the dominant (002) peak were calculated using the equations [19, 25, 26]:

$$2d\sin\theta = n\lambda, \tag{2}$$

Table 2. Surface topographic parameters of CdS thin films obtained at different deposition times

Parameters	$t = 5$ min	$t = 10$ min	$t = 15$ min
R_a, nm	9.2	5.2	6.9
R_{rms}, nm	12.8	6.8	9.1
R_{sk}	1.16	0.52	0.71
R_{ku}	6.36	3.84	5.18

Table 3. Calculated structural parameters of CdS thin films based on the (002) H peak data

Sample	(002) Peak Position, 2θ, deg	FWHM, β, deg	Crystallite Size, *L*, nm	Dislocation Density, $\delta \times 10^{-3}$ m^{-2}	Microstrain, $\varepsilon \times 10^{-3}$	Lattice Parameters		
						a, Å	*c*, Å	*c*/*a*
CS5	26.42	1.063	10.29	9.401	4.73	3.981	6.533	1.64
CS10	26.64	1.062	10.31	9.401	4.59	4.051	6.610	1.63
CS15	26.60	1.084	10.11	9.791	4.91	4.121	6.610	1.62

$$\frac{1}{d^2} = \frac{4}{3}\left(\frac{h^2 + hk + k^2}{a^2}\right) + \frac{l^2}{c^2}, \tag{3}$$

$$\varepsilon = (\beta \cos\theta)/4, \tag{4}$$

$$\delta = \frac{1}{L^2}. \tag{5}$$

Here, h, k, l are the Miller indices.

It is well known that CdS has two crystalline structures: a metastable cubic phase (zinc blende) and a highly stable hexagonal phase (wurtzite), which can form during the CBD process depending on the growth conditions. We found that for all samples CS5, CS10, and CS15, an intense diffraction peak is observed at a Bragg angle (2θ) of about 26.5°, corresponding to the (002) plane of the hexagonal phase of CdS (H) or the (111) plane of the cubic phase (C). However, the appearance of peaks corresponding to the (110)H plane at around 44.4° and the (112)H plane at around 52.2° indicates that the crystalline structure of the films belongs to the hexagonal phase or represents a mixture of hexagonal and cubic phases. The absence of other phases indicates the high quality of the synthesized thin films. The diffractograms also show that the intensity and height of the dominant (002)H peak at 26.5°, as well as the (110)H and (112)H peaks at around 44.4° and 52.2°, respectively, increase with longer deposition times. This is associated with an increased amount of deposited material, which in turn leads to an increase in the thickness of the CdS film.

The position of the (002)H peak at 2θ = 26.42° for films deposited for 5 minutes shifts toward higher angles, reaching 26.64° as the deposition time increases to 15 minutes. This indicates the stable formation of the crystalline structure of CdS films even at a relatively short deposition time (5 min).

Table 3 presents the results of the structural parameter calculations based on the (002)H peak data, performed using the FullProf program. The hexagonal crystal lattice of the synthesized CdS films was confirmed according to JCPDS data No. 80-0006, with lattice constants: $a = 4.1002$ Å, $c = 6.6568$ Å, and $c/a = 1.62$, which are in good agreement with the calculated values shown in Table 3.

As already noted above, there is some discrepancy between the average size estimates of structural elements obtained from SEM, AFM, and the Scherrer formula based on XRD data, with the latter typically yielding sizes several times smaller. This apparent inconsistency arises because SEM and AFM cannot reveal the substructures of the polycrystalline film; they provide the average grain (cluster) size, which in turn consists of smaller crystallites distributed throughout the film volume. It is the smallest size of these crystallites that is detected in XRD analysis [27, 28].

3.5. Raman Spectroscopy

Figure 5a shows the Raman spectra of CdS thin films deposited on PI substrates. Table 4 presents the frequencies and full width at half maximum (FWHM) values of the observed scattering peaks, obtained from measurements at two different locations on the samples. Each spectrum has three peaks: an intense peak at approximately 302 cm^{-1} corresponding to the first-order longitudinal optical mode (1LO), accompanied by second-order (2LO) and third-order (3LO) overtones at approximately 604 and 912 cm^{-1}, respectively.

It should be noted that in the Raman spectra of bulk CdS samples with a wurtzite structure, the dominant 1LO phonon peak at 305 cm^{-1} and its first overtone at 611 cm^{-1} are also frequently observed [6, 29].

As a result of the decomposition of the Raman scattering spectrum of the CS10 film using Gaussian functions (Fig. 5b), it was established that the asymmetric 1LO peak in the region of approximately 302 cm^{-1} consists of several components with maxima at 254, 289, 302, 335, and 392 cm^{-1}. The components of the scattering spectrum observed below 302 cm^{-1} are interpreted by various authors as the presence of surface phonons (SP) and/or transverse optical phonons (TO) [30–33].

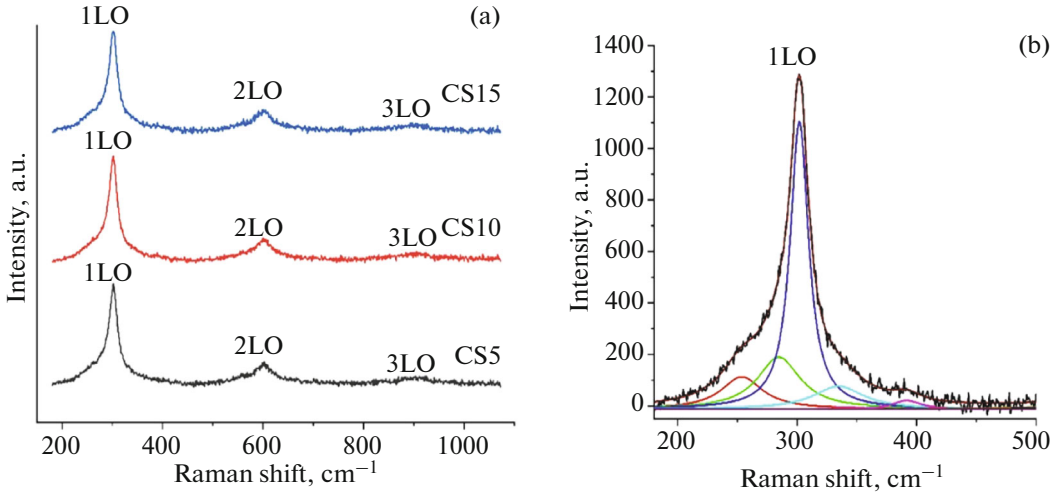

Fig. 5. (a) Raman spectra of CdS thin films obtained at different deposition durations, and (b) deconvolution of the 1LO peak for the CS10 sample.

It is known that in films thicker than 100 μm, in the backscattering geometry where the z-axis is directed perpendicular to the (001) surface of the sample, according to selection rules, only longitudinal optical (LO) phonons can be observed in the Raman spectra. In contrast, transverse optical (TO) and surface phonon modes usually do not appear due to symmetry restrictions and their low intensity [30]. Accordingly, if additional components are observed in the Raman spectra of thin CdS films, it can be assumed that these are nanostructured films, in which surface and confined phonon modes, LO and TO phonon modes of the cubic phase of CdS, and so on, may be present [34, 35].

A slight (~2–3 cm^{-1}) shift of the modes toward lower frequencies relative to the 1LO mode of the bulk CdS sample is likely caused by strain effects or spatial confinement of phonons. It is also known that mechanical stresses occurring at the film–substrate interface can cause the observed peak shifts [33]. However, since all deposition processes were carried out at the same temperature and on substrates of the same type, this effect can be neglected.

3.6. Optical Properties

Figure 6 shows the transmission (T) and reflection (R) spectra of thin CdS films in the wavelength range from 420 to 1020 nm. The synthesized samples demonstrate a high transmission coefficient (up to 80–95%) and a low reflection coefficient (less than 9%) in the visible and near-infrared regions of the spectrum, as well as a sharp optical edge around ~520 nm. The high transparency and absence of interference fringes in all CdS films indicate significant light scattering during interaction with the film, caused by surface roughness and inhomogeneity.

Table 4. Frequency and Full Width at Half Maximum (FWHM) of Raman Modes of thin CdS films

Sample	1LO		2LO		3LO	
	Peak Frequency, cm^{-1}	FWHM, cm^{-1}	Peak Frequency, cm^{-1}	FWHM, cm^{-1}	Peak Frequency, cm^{-1}	FWHM, cm^{-1}
CS5	302	20.9	604	25.5	912	–
	302	20.3	603	27.9	912	–
CS10	302	21.5	603	28.1	912	–
	303	21.6	604	30.9	913	–
CS15	302	20.1	604	23.6	917	–
	302	20.6	605	28.8	916	–

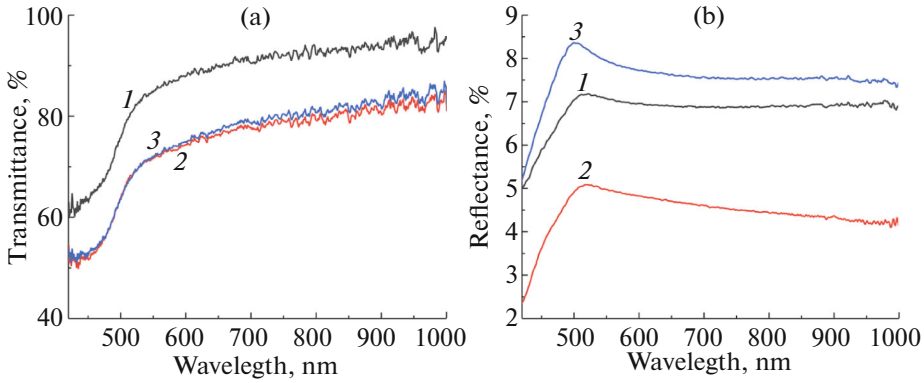

Fig. 6. (a) Transmission and (b) reflection spectra of CdS films at different deposition times: (*1*) CS5; (*2*) CS10; (*3*) CS15.

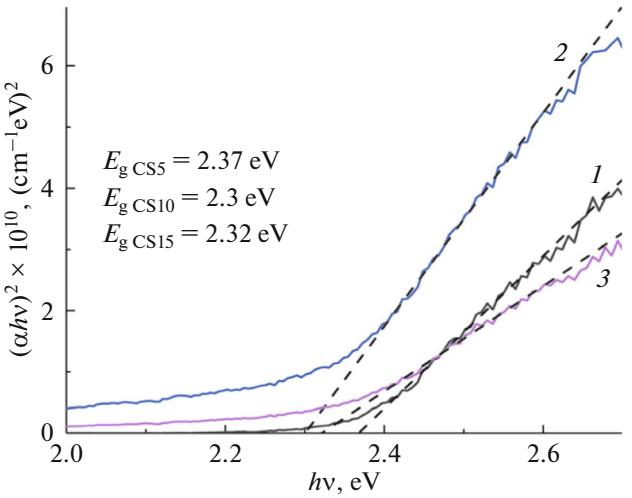

Fig. 7. Optical band gap width of CdS films calculated using Tauc method for: (*1*) CS5; (*2*) CS10; (*3*) CS15.

Based on the transmission and reflection spectra, the absorption coefficient (α) was calculated taking into account multiple internal reflections within the plane-parallel sample at the interface boundaries, according to the expression [18]:

$$\alpha = -\frac{1}{d}\ln\left(\frac{\sqrt{(1-R)^4 + 4T^2R^2} - (1-R)^2}{2TR^2}\right), \quad (6)$$

where d is the film thickness, T and R are the light transmission and reflection coefficients, respectively.

The optical band gap (E_g) of CdS films can be estimated by assuming the presence of direct allowed transitions between the valence band and the conduction band, using the dependence $(\alpha h\nu)^2 = A(h\nu - E_g)$ for the intrinsic light absorption coefficient as a function of photon energy, where A is a constant and $h\nu$ is the photon energy. By extrapolating the linear portion of the $(\alpha h\nu)^2 = f(h\nu)$ plot to the photon energy axis, according to Tauc method, the band gap was determined to be 2.37, 2.30, and 2.32 eV for the CS5, CS10, and CS15 films, respectively (Fig. 7). This non-monotonic variation in the band gap may be caused by several factors [4, 14], but in our case, it is apparently due to a change in the stoichiometry of the synthesized films. As the deposition time increases from 5 to 15 minutes, the Cd/S ratio first increases from 0.39 to 0.78, then decreases to 0.7 (see Table 1).

The quality of polycrystalline CdS thin films, in terms of their photoelectric properties, is largely determined by the presence of recombination centers associated with impurities, lattice defects, grain boundary, and surface states, and can be assessed through the study of their photoluminescence (PL). In addition, such studies provide information about localized energy states caused by deviations from stoichiometry, which lead to the formation of vacancies or interstitial cadmium and/or sulfur atoms. These defects are mainly

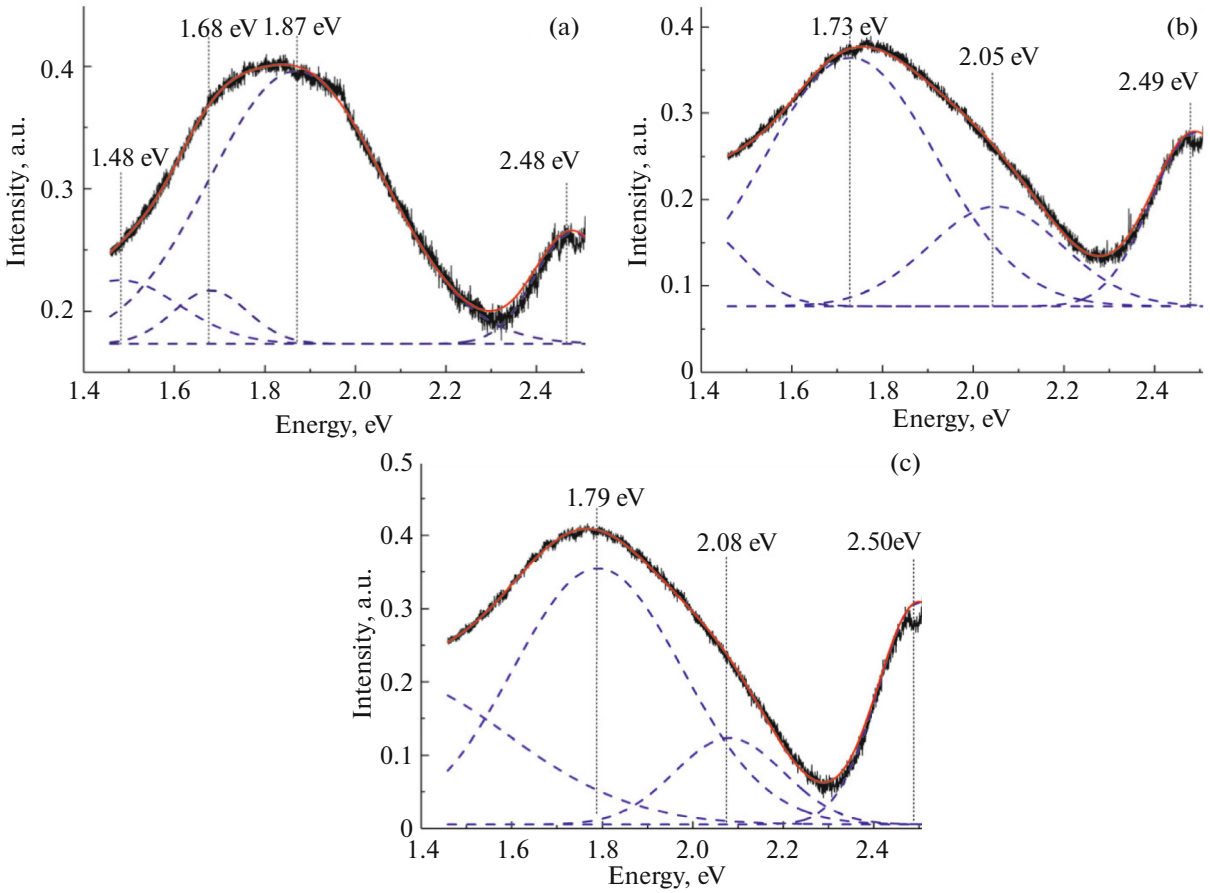

Fig. 8. PL spectra of CdS films after background subtraction of the PI substrate emission and their peak deconvolutions: (a) CS5; (b) CS10; (c) CS15.

responsible for the radiative recombination of nonequilibrium charge carriers. There are many studies on the PL of CdS crystals and films [36, 37]. It is known that the PL emission bands observed in the photon energy range of 2.18–2.54 eV (close to the band gap of CdS) are called "green" bands. Emission bands in the range of 2.07–2.18 eV are usually referred to as "yellow" bands, the "orange" band is located in the range of 2.00–2.07 eV, and PL observed in the range of 1.54–2.00 eV is referred to as "infrared/red" emission.

Figure 8 shows the PL spectra of CdS thin films deposited at a constant temperature (62°C) for various durations ranging from 5 to 15 min.

The recorded PL spectra for all deposited CdS films (after subtracting the background emission from the PI substrate) exhibit two main peaks: a "green" peak at a photon energy of approximately 2.49 eV and a broad "red" peak with a maximum near 1.75 eV. It should be noted that similar PL spectra have been reported in many other studies for polycrystalline CdS layers grown by the CBD method on various substrates [36, 37].

When interpreting the obtained spectra, it should be taken into account that the CdS films were not intentionally doped, and the films likely contain intrinsic defects caused by deviations from ideal stoichiometry. EDS results indicate sulfur enrichment in the samples, which may suggest the presence of dominant acceptor levels associated with interstitial sulfur atoms or cadmium vacancies.

The red PL band clearly shows a substructure. Peak decomposition and approximation using a sum of individual Gaussian-shaped bands [38] revealed several emission sub-bands concentrated in the energy regions indicated in Fig. 8.

The origin of the infrared PL peak at 1.48 eV is assumed, as suggested in [37], to be associated with isolated Cd vacancies. The red emission sub-band in the range of 1.68–1.79 eV is attributed to electron transitions from the conduction band to acceptor levels of interstitial sulfur atoms [4, 36, 37]. The yellow subband in the range of 1.87–2.08 eV is likely due to radiative transitions of electrons from donor levels to acceptor levels, indicating a donor–acceptor recombination mechanism. It is worth noting that the posi-

tion of the green emission peak near 2.48–2.50 eV, within the range of the average thermal energy, coincides with the optical band gap value of polycrystalline CdS. This band may be associated with radiative transitions of free electrons from the conduction band to the valence band, or with transitions from shallow donor levels to the valence band. The presence of an intense green emission band in the PL spectra indicates better crystallinity of the material synthesized over a longer deposition time, which is characterized by fewer grain boundaries and a minimal density of intrinsic defects.

4. CONCLUSION

CdS thin films with good structural and morphological quality were successfully synthesized on PI substrates using the CBD method at various deposition times without any post-growth treatment. The obtained polycrystalline films are characterized by cadmium deficiency, a hexagonal structure with a preferred orientation along the (002) direction, and crystallite sizes ranging from 10.1 to 10.3 nm.

SEM images show a dense structure with a relatively smooth, void-free surface without holes or cracks; the grain size ranges from 124 to 132 nm. The root mean square roughness of the CdS films, determined by AFM, is in the range of 9–13 nm, indicating compactness and uniform grain distribution.

The Raman scattering spectra revealed three peaks corresponding to the optical 1LO lattice vibration mode of CdS and its overtones, 2LO and 3LO. The optical band gap of the films was in the range of 2.30–2.37 eV, and their transmittance in the visible range was between 80 and 95%. The PL spectra of all CdS thin films deposited on PI substrates showed a relatively narrow peak at 2.49 eV (green emission band) and a broad defect-related emission band with a maximum of 1.75 eV (red emission band). As the deposition time increases, the intensity ratio of the green to red peaks also increases, which confirms the improvement in the crystallinity of the material.

The main conclusion of this work is that the CBD method, at a relatively low temperature (62°C), enables the growth of high-crystalline-quality CdS thin films on PI substrates. We believe that this low-cost technology offers promising opportunities for the deposition of thin layers on various flexible substrates suitable for use in flexible solar cells and optoelectronic devices.

FUNDING

This work was supported by the Science Committee of the Ministry of Education, Science, Culture, and Sports of the Republic of Armenia (grant No. 21 SC-BRFFR-1C003) and the Belarusian Foundation for Basic Research (grant No. T21ARM-003).

CONFLICT OF INTEREST

The authors of this work declare that they have no conflicts of interest.

REFERENCES

1. Jie, L., Gao, X., Cao, X., Wu, Sh., Long, X., Ma, Q., and Su, J., *Mater. Sci. Semicond. Process.*, 2024, vol. 176, p. 108288.
2. Vigil-Galán, O., Pulgarín, F.A., Cruz-Gandarilla, F., Courel, M., Villarreal-Ruiz, G., Sanchez, Y., Jimenez-Olarte, D., and Saucedo, E., *Materials and Design*, 2016, vol. 99, p. 254.
3. Maricheva, J., Bereznev, S., Naidu, R., Maticiuc, N., Mikli, V., and Kois, J., *Mater. Sci. Semicond. Process.*, 2016, vol. 54, p. 14.
4. Hariech, S., Bougrida, J., Belmahi, M., Medjahdi, G., Aida, M.S., and Zertal, A., *Bull. Mater. Sci.*, 2022, vol. 45, p. 78.
5. Abbas, K., Muhammad, A., Mehmood, R.F., Sher, M., and Akhtar, J., *Mater. Today*, 2022, vol. 53, p. 339.
6. Oladeji, I.O., Chow, L., Liu, J.R., Chu, W.K., Bustamante, A.N.P., Fredricksen, C., and Schult, A.F., *Thin. Sol. Films*, 2000, vol. 359, p. 154.
7. Lakmal, A.A.I., Kumarasinghe, R.K.K.G.R.G., Seneviratne, V.A., Chen, J-Y., Song, J-M., and Dassanayake, B.S., *Mater. Sci. Engin.: B*, 2021, vol. 273, p. 115406.
8. Jassim, S., Abbas, A.M., Al-Shakban, M., and Ahmed, L.M., *Egypt. J. Chem.*, 2021, vol. 64, p. 2533.
9. Martínez-Landeros, V.H., Hernandez-Como, N., Gutierrez-Heredia, G., Quevedo-Lopez, M.A., and Aguirre-Tostado, F.S., *Thin Solid Films*, 2019, vol. 682, p. 24.
10. Das, N.K., Chakrabartty, J., Fahrad, S.F.U., Sen Gupta, A.K., Ikball Ahamed, E.M.K., Rahman, K.S., Wafi, A., Alkahtani, A.A., Matin, M.A., and Amin, N., *Results in Physics*, 2020, vol. 17, p. 103132.
11. Paudel, N.R., Xiao, Ch., and Yan Y., *J. Mater. Sci.: Mater. Electron.,* 2014, vol. 25, p. 1991.

12. Tsuji, M., Aramoto, T., Ohyama, H., Hibino, T., and Omura K., *Jpn. J. Appl. Phys.,* 2000, vol. 39, p. 3902.
13. Faraj, M.G., Eisa, M.H., and Pakhuruddin M.Z., *Int. J. Electrochem. Sci.,* 2019, vol. 14, p. 10633.
14. Rodríguez-Rosales, K., Quiñones-Galván, J.G., Guillén-Cervantes, A., Campos-González, E., Santos-Cruz, J., Mayén-Hernández, S.A., Arias-Ceron, J.S., de la L Olvera, M., Zelaya-Angel, O., Hernández-Hernández, L.A., Contreras-Puente, G., and de Moure-Flores, F., *Mater. Res. Express*, 2017, vol. 4, p. 075904.
15. Ouafi, M., Jaber, B., and Laanab, L., *Superlattices and Microstructures,* 2019, vol. 129, p. 212.
16. Park, Y., Kim, E.K., Lee, S., and Lee, J., *J. Nanosc. Nanotechn*., 2014, vol. 14, p. 3880.
17. Li, X., Li, P., Wu, Zh., Luo, D., Yu, H-Y., and Lu, Zh-H., *Mater. Rep. Lett.*, 2021, vol. 1, p. 100001.
18. Gremenok, V.F., Zaretskaya, E.P., Stanchik, A.V., Buskis, K.P., Pashayan, S.T., Tokmajyan, A.S., Musayelyan, A.M., and Petrosyan, S.G., *Optics and Spectroscopy*, 2024, vol. 132, p. 145.
19. Ashok, A., Regmi, G., Romero-Núñez, A., Solis-López, M., Velumani, S., and Castaneda, H., *J. Mater. Sci.: Mater. Electron.,* 2020, vol. 31, p. 74996.
20. Rahman, F., Hossain, J., and Ismail, A.B. Md., *SN Appl. Sci.,* 2020, vol. 2, p. 1956.
21. Gadelmawla, E.S., Koura, M.M., Maksoud, T.M.A., Elewa, L.M., and Soliman, H.H., *J. Mater. Proces. Techn*., 2002, vol. 123, p. 133.
22. Lisco, F., Kaminski, P.M., Abbas, A., Bass, K., Bowers, J.W., Claudio, G., Losurdo, M., and Walls, J.M., *Thin Solid Films*, 2015, vol 582, p. 323.
23. Dissanayake, D.M.C.U.Ch. and Samarasekara, P., *J. Sci. Univ. Kelaniya,* 2015, vol 10, p. 13.
24. Warren, B.E., *X-ray Diffraction*, New York, Dover Publications, 1990.
25. Williamson, G.K. and Smallman, R.E., *Phil. Mag.*, 1956, vol. 1, p. 34.
26. Rasool, S., Saritha, K., Reddy, K.T.R., Tivanov, M.S., Gremenok, V.F., Zimin, S.P., Pipkova, A.S., Mazaletskiy, L.A., and Amirov, I.I., *Mater. Res. Express*, 2020, vol. 7, p. 016431.
27. Chowdhury, R.I., Hossen, M.A., Mustafa, G., Hussain, S., Rahman, S.N., Farhad, S.F.U., Murata, K., Tambo, T., and Islam, A.B.M.O., *Intern. J. Modern Phys*., 2010, vol. 24, p. 5901.
28. Acharya, K.P., Skuza, J.R., Lukaszew, R.A., Liyanage, C., and Ullrich B., *J. Phys.: Condens. Matter*, 2007, vol. 19, p. 196221.
29. Trajić, J., Gilić, M., Romčević, N., Romčević, M., Stanišić, G., Hadžić, B., Petrovic, M., and Yahia, Y.S., *Sci. Sinter*., 2015, vol. 47, p. 145.
30. Saleem, M.F., Zhang, H., Deng, Y., and Wang, D., *J. Raman Spectrosc*., 2016, vol. 48, p. 224.
31. Prasad, M.V.V., Thyagarajan, K., and Kumar, B.R., *IOP Conf. Series: Materials Science and Engineering*, 2016, vol. 149, p. 012051.
32. Chi, T.T.K., Gouadec, G., Colomban, Ph., Wang, G., Mazerolles, L., and Liem, N.Q., *J. Raman Spectrosc*., 2011, vol. 42, p. 1007.
33. Keshav, R., Rao, A., and Mahesha, M.G., *Opt. Quant. Electron*., 2018, vol. 50, p. 186.
34. Arora, A.K., Rajalakshmi, M., Ravindran, T.R., and Sivasubramanian, V., *J. Raman Spectrosc*., 2007, vol. 38, p. 604.
35. Zaretskaya, Ye.P., Gremenok, V.F., Buskis, K.P., Korolik, O.V., Pashayan, S.T., Tokmadzhyan, A.S., Musayelyan, A.S., and Petrosyan S.G., *Zhurnal Priklad. Spektrosk*., 2024, vol. 91, p. 32.
36. Aguilar-Hernandez, J., Sastre-Hernandes, J., Ximello-Quiebras, N., Mendoza-Perez, R., Vigil-Galan, O., Contreras-Puente, G., and Cardenas-Garcia M., *Thin Sol. Films*, 2006, vol. 511-512, p. 143.
37. Abken, A.E., Halliday, D.P., and Durose, K., *J. Appl. Phys*., 2009, vol. 105, p. 064515.
38. Kovalenko, A.V., Vovk, S.M., and Plakhtii, Ye.G., *J. Appl. Spectrosc*., 2021, vol. 88, p. 357.

Translated by T. Azatian